Published OnlineFirst October 21, 2013; DOI: 10.1158/0008-5472.CAN-13-1657

miRNA-95 Mediates Radioresistance in Tumors by Targeting the Sphingolipid Phosphatase SGPP1

Xiaoyong Huang[1], Samira Taeb[1], Sahar Jahangiri[1], Urban Emmenegger[1,2], Elisa Tran[1], Jeff Bruce[3,5], Aruz Mesci[1], Elina Korpela[1,3], Danny Vesprini[1,4], C. Shun Wong[1,3,4], Robert G. Bristow[3,4,5], Fei-Fei Liu[3,4,5], and Stanley K. Liu[1,3,4]

Abstract

Radiation resistance poses a major clinical challenge in cancer treatment, but little is known about how microRNA (miR) may regulate this phenomenon. In this study, we used next-generation sequencing to perform an unbiased comparison of miR expression in PC3 prostate cancer cells rendered resistant to fractionated radiation treatment. One miR candidate found to be upregulated by ionizing radiation was miR-95, the enforced expression of which promoted radiation resistance in a variety of cancer cells. miR-95 overexpression recapitulated an aggressive phenotype including increased cellular proliferation, deregulated G_2–M checkpoint following ionizing radiation, and increased invasive potential. Using combined *in silico* prediction and microarray expression analyses, we identified and validated the sphingolipid phosphatase SGPP1, an antagonist of sphingosine-1-phosphate signaling, as a target of miR-95 that promotes radiation resistance. Consistent with this finding, cell treatment with FTY720, a clinically approved small molecule inhibitor of S1P signaling, sensitized miR-95 overexpressing cells to radiation treatment. *In vivo* assays extended the significance of these results, showing that miR-95 overexpression increased tumor growth and resistance to radiation treatment in tumor xenografts. Furthermore, reduced tumor necrosis and increased cellular proliferation were seen after radiation treatment of miR-95 overexpressing tumors compared with control tumors. Finally, miR-95 expression was increased in human prostate and breast cancer specimens compared with normal tissue. Together, our work reveals miR-95 expression as a critical determinant of radiation resistance in cancer cells. *Cancer Res; 73(23); 6972–86. ©2013 AACR.*

Introduction

Although radiation is an effective, well-established cancer treatment modality, patients can develop cancer recurrence after treatment. Recurrent tumors tend to display a more aggressive phenotype including increased proliferation and acquisition of a higher tumor grade, which clinically manifests as larger tumors that are typically associated with lymph node metastases, and a worse prognosis (1–3). Thus, improvements are essential to increase the effectiveness of radiation treatment in killing cancer cells and minimize the risk of recurrent disease.

The study of microRNAs (miR) is a promising and emerging research area due to their potential ability to simultaneously regulate multiple oncogenic pathways that may influence radiation response (4). However, research is needed to clearly elucidate the role of specific miR in tumor response to ionizing radiation. miRs are short, noncoding single-stranded RNA that can decrease the expression of hundreds of downstream genes (5). They accomplish this function primarily by binding to the 3′ untranslated (3′UTR) region of mRNA transcripts, and depending on their degree of complementarity (degree of base pair matching within the 3′UTR region), this binding results in either transcript degradation or inhibition of translation. At least 50% of the annotated miRs are known to be located within fragile sites of the genome that are associated with cancer (6). The dysregulated expression of miR is believed to be involved in the pathogenesis of cancer (7). A single miR can potentially regulate several hundred genes, thus its dysregulated expression can influence a broad range of cancer-related processes including proliferation, apoptosis, angiogenesis, invasion, and metastasis. Some miRs are important mediators of tumorigenesis when overexpressed, whereas others can function as tumor suppressors and thus promote tumorigenesis when underexpressed (7). Despite the knowledge that miR are involved in cancer development and progression, very little is known about their role in tumor response to cancer therapies.

The discovery that miR may play a role in the cellular response to ionizing radiation is a relatively recent finding (8–11). Their expression profile can change within minutes to hours following ionizing radiation, and induction of many miR have been reported to be linked to activation of a key DNA

Authors' Affiliations: [1]Sunnybrook Research Institute, Sunnybrook Health Sciences Centre; Departments of [2]Medicine, [3]Medical Biophysics, and [4]Radiation Oncology, University of Toronto; and [5]Ontario Cancer Institute, University Health Network, Toronto, Canada

Note: Supplementary data for this article are available at Cancer Research Online (http://cancerres.aacrjournals.org/).

Corresponding Author: Stanley K. Liu, 2075 Bayview Avenue, Rm T2-142, Sunnybrook Health Sciences Centre, Toronto, Ontario, M4N 3M5, Canada. Phone: 416-480-4998; Fax: 416-480-6002; E-mail: stanley.liu@sunnybrook.ca

doi: 10.1158/0008-5472.CAN-13-1657

Published OnlineFirst October 21, 2013; DOI: 10.1158/0008-5472.CAN-13-1657

damage sensor, ataxia telangiectasia mutated (ATM) kinase (12). Although studies have confirmed the role of several miR (let-7, miR-21, and miR-34) in regulating radiosensitivity (reviewed in ref. 10), it is unknown whether other miR may mediate response to ionizing radiation. The identification of putative miR involved in the response to ionizing radiation has largely been through miR array expression profiling from cells treated with ionizing radiation, yet this approach may be limited by the number of miR that are present on the miR array. Some studies have also tested miR based on their predicted regulation of genes implicated in resistance to ionizing radiation such as EGFR (13) or ATM (14), which relies on prior knowledge of predicted target genes. To address these limitations, we generated radiation-resistant human PC3 prostate cancer cells (PC3 rad res) via fractionated ionizing radiation, which we believed would be enriched for miR important in the radiation response. Then, we utilized next-generation sequencing to comprehensively identify miR that may be involved in radiation response. We focused on one of these candidates, miR-95, because its potential role in radiation response had not yet been characterized. Previously, it has been reported that miR-95 expression is upregulated in human colorectal and pancreatic carcinoma samples compared with normal controls (15, 16), and its overexpression promoted tumor growth (15, 17). We demonstrate in this study that miR-95 overexpression promotes radiation resistance in prostate and breast cancer cells and in human xenograft tumors. We identify sphingosine-1-phosphate phosphatase 1 (SGPP1) as a novel target of miR-95 that can induce radiation resistance. In addition, we show that miR-95 overexpression results in an aggressive phenotype with increased proliferation, invasiveness, and anchorage-independent growth that mimics findings seen in our radiation-resistant PC3 cancer model. Together, our research provides novel insights into the role of miR-95 in cancer aggression and resistance to ionizing radiation.

Materials and Methods

Cell lines and cell culture

Human prostate adenocarcinoma (PC3, DU145) and human breast adenocarcinoma (MDA-MB-231) cell lines were purchased from American Type Culture Collection. Early passage cell lines were cultured in Dulbecco's Modified Eagle Medium (DMEM) containing 4.5 g/L glucose (Invitrogen) supplemented with 10% FBS (Invitrogen) and penicillin (100 U/mL)—streptomycin (100 μg/mL; Invitrogen; hereafter referred to as 10% DMEM), and maintained in a humidified 37°C incubator with 5% CO_2. MCF10A immortalized human mammary epithelial cells were kindly provided by Dr. Senthil Muthuswamy (Ontario Cancer Institute, University of Toronto, Toronto, Ontario), and cultured in DMEM/F12 supplemented with 5% horse serum (Invitrogen), EGF (20 ng/mL), (Sigma-Aldrich) hydrocortisone (0.5 mg/mL; Sigma-Aldrich), cholera toxin (100 ng/mL; Sigma-Aldrich), insulin (10 μg/mL; Sigma-Aldrich), and penicillin–streptomycin (Invitrogen). Cell lines were passaged when they reached approximately 80% confluency and were regularly tested with MycoAlert (Lonza) to ensure the absence of mycoplasma contamination.

Generation of radiation-resistant PC3 prostate cancer cells

The radiation-resistant PC3 cells were generated by treatment with mock irradiation (i.e., parental cells) or ionizing radiation (i.e., rad res cells) delivered using 110 kV X-rays from a Faxitron 43855F (Faxitron Bioptics LLC) for a daily 2 Gy dose administered 5 days per week, followed by a 7- to 10-day recovery, with this process repeated for a total of 45 treatments totaling 90 Gy.

Next-generation sequencing

Total RNA was extracted from cells using the mirVana miRNA Isolation Kit (Life Technologies). The RNA integrity (RNA integrity number $\geq$ 6.0) was determined using the Agilent 2100 Bioanalyzer with the RNA 6000 Nano kit (Agilent Technologies Canada Inc.). Small RNA fraction was enriched from total RNA using the Purelink miRNA Isolation Kit (Life Technologies). The percentage of miR (10–40 nt) in the small RNA fraction (~200 nt) was estimated using the Agilent 2100 Bioanalyzer with the small RNA kit. Small RNA libraries were constructed using the Applied Biosystems SOLiD Total RNA-Seq Kit (Life Technologies) with the SOLiD RNA Barcoding Kit (Life Technologies). SOLiD adaptors were hybridized and ligated to 100 ng of small RNA and then reverse transcription was performed to generate cDNA libraries. cDNA products between 60 and 80 bp were excised from a 10% TBE-urea gel followed by PCR amplification (15 cycles) with barcode primer using the SOLiD RNA Barcoding Kit. The concentration and quality of cDNA libraries were quantitated using the Qubit 2.0 Fluorometer with Qubit dsDNA HS Assay Kit (Life Technologies) and the Agilent 2100 Bioanalyzer with the High Sensitive DNA Kit. Bar-coded cDNA libraries were pooled together in equal concentrations in one pool and driven onto beads to generate bead clones by emulsion PCR. The 3′ modified beads were then deposited onto a Flowchip. 35 bp single-end sequence reads were generated using the Applied Biosystems SOLiD5500xl sequencer. The sequencing data were analyzed by Genesifter analysis edition version v4.0 (Geospiza Inc.). Non-miR reads such as transfer RNA and small nuclear RNA were depleted from the sequenced data. The remaining sequencing data were then mapped onto Human reference sequence, NCBI Build 36. Normalized expression level (reads per million, RPM) was calculated for known small RNA (the miRBase sequence database, http://www.mirbase.org/). GeneSifter Analysis Edition v4.0 was used to identify miR that were increased by at least 2.0-fold in the PC3 rad res cells compared with PC3 parental cells, and with a minimum expression level of 100 in the PC3 control cells.

Transfection of miR mimics and siRNA

A total of 3×10^5 cells were seeded into 6-well plates, then 16 hours later, miScript miRNA miR-95 mimic or miR control mimic (Thermo Fisher Scientific) were mixed with 6 μL of DharmaFECT transfection reagent (Thermo Fisher Scientific) and DMEM as per the manufacturer's instructions, then added to 10% DMEM for transfection of the cells. For siRNA transfection, control or siRNA for DICER1, PTPN21, SGPP1, or UBE4E (Santa Cruz Biotechnology) transiently transfected into

Published OnlineFirst October 21, 2013; DOI: 10.1158/0008-5472.CAN-13-1657

PC3 cells using Lipofectamine 2000 (Invitrogen) as per manufacturer's recommendations, and 24 hours later, radiation clonogenic survival assays (described later) were performed on the transfected cells.

Generation of stable overexpressing miR-95 cell lines

Cells were transduced with shMIMIC miR-95 or nonsilencing control lentiviral particles as per manufacturer's instructions (ThermoScientific), selected using puromycin for 2 weeks, and stable transductants were pooled.

Cellular proliferation assay

Cells were seeded in triplicate (0.5×10^5 cells/well for mock ionizing radiation, and 1.0×10^5 for 6 Gy ionizing radiation) in 10% DMEM in 6-well plates and were mock irradiated or irradiated with a 6 Gy dose of ionizing radiation 6 hours later. Four days later, cells were trypsinized and total viable cell number determined using the Countess automated cell counter (Life Technologies). For chemotherapy treatment experiments, PC3 parental or rad res cells were seeded (1×10^3 cells/well) in a 96-well plate in 10% DMEM overnight, and the following morning, chemotherapy-containing culture media was added at increasing concentrations (cisplatin and docetaxel were obtained from the Sunnybrook Odette Cancer Centre pharmacy). After 72 hours of incubation, the number of viable cells was quantified by the MTS assay (CellTitre 96 AQ_{ueous} Cell Proliferation Assay; Promega Corporation) according to the manufacturer's instructions, and absorbance at 490 nm was measured using the Benchmark Plus multiwell plate reader (Bio-Rad Laboratories Inc.).

Cell-cycle analysis

Cells were mock irradiated or irradiated with a 6 Gy dose of ionizing radiation, then 24 hours later, cells were trypsinized, washed in PBS, and fixed in ice-cold 80% ethanol in Hank's Buffered Salt Solution (HBSS; 137 mmol/L NaCl, 5.4 mmol/L KCl, 0.25 mmol/L Na_2HPO_4, 0.44 mmol/L KH_2PO_4, 1.3 mmol/L $CaCl_2$, 1.0 mmol/L $MgSO_4$, 4.2 mmol/L $NaHCO_3$) for 30 minutes on ice. Fixed cells were collected by centrifugation, washed twice with PBS, and resuspended in 50 μg/mL propidium iodide (Sigma-Aldrich) with 0.6% NP-40 (Thermo Fisher Scientific) and 0.1 mg/mL RNAse A in HBSS for 30 minutes at room temperature in the dark. Cells were then collected by centrifugation, resuspended in PBS, and 20,000 events captured on a FACSCalibur flow cytometer (BD Biosciences) and cell-cycle profile analyzed using FlowJo 10.0.4 (Tree Star Inc.).

Radiation clonogenic survival assay

Cells were seeded at 250, 500, 2,000, and 4,000 cells per well onto a six-well plate in 10% DMEM in triplicate and mock irradiated (0 Gy) or irradiated with 2, 4, or 6 Gy dose of ionizing radiation, respectively. Then cells were placed in a humidified CO_2 incubator at 37°C to allow colonies to form. Colonies were stained with crystal violet staining solution [0.5% crystal violet (Sigma-Aldrich), 25% methanol] and counted. Survival was expressed as the relative plating efficiencies of the treated cells compared with that of the mock-irradiated cells. The experiments were performed 3 separate times. Radiation dose–response curves were created by fitting the data to the linear quadratic equation $S = e^{-\alpha D - \beta D2}$ using GraphPad Prism 5.0 (GraphPad Software Inc.), where S is the surviving fraction, α and β are inactivation constants, and D is the dose in Gy. The area under the curves (AUC) that represent the mean inactivation dose (MID) were also calculated using GraphPad Prism. The radiation protection factor (RPF) was calculated by dividing the MID of the test cells by the MID of control cells.

Cellular senescence assay

Cells were seeded into 6-well plates and 16 hours later, mock irradiated or irradiated with a 6 Gy dose of ionizing radiation, then 4 days later, fixed and stained for senescence-associated β-galactosidase using the senescence-associated β-galactosidase staining kit (Cell Signaling Technology) as per manufacturer's recommendations. The percentage of β-galactosidase stained cells was determined by counting a minimum of 250 cells.

Real-time quantitative PCR

For miR expression, total miR was extracted from cells or tumors using the mirVana miRNA kit (Invitrogen) according to the manufacturer's instructions. cDNA was synthesized using the miScript II RT kit (Qiagen) as per manufacturer's instructions. The mature miR-95 expression level was quantified through quantitative real-time PCR (qRT-PCR) using the miScript SYBR Green PCR Kit (Qiagen) and miScript Primer Assay for SNORD61 and miR-95 (Qiagen) on the StepOnePlus Real-time PCR system (Life Technologies). For gene expression, RNA was extracted using the RNeasy Mini Kit (Qiagen) and cDNA synthesized using Omniscript RT Kit (Qiagen) as per manufacturer's instructions. SGPP1, DICER1, UBE4B, and PTPN21 expression levels were quantified through qRT-PCR using the QuantiTect SYBR Green PCR Kit (Qiagen) on the StepOnePlus Real-time PCR system. For both miR and mRNA, expression levels were calculated using the comparative Ct method via StepOne Software (Life Technologies), and relative expression levels normalized to SNORD61 (for miR) or GAPDH (for mRNA). Primer sequences: SGPP1: forward 5′-ATGGTCCTCCTCACCTATGG-3′, reverse 5′-TCAATCAGGTCCACAAATGG-3′; UBE4B: forward 5′-TCGCCCTCTAATAGCCTTGA-3′, reverse, 5′-TATCACTGAGGCTCCGCTTT-3′; DICER1: forward 5′-ACCAACATTTTGTGCGGAAT-3′, reverse, 5′-TGCTTCCATCTGTTTGTTGC-3′; PTPN21: forward 5′-CGGTGGGTAGATTTGGAAAA-3′, reverse 5′-ACCAAAATCCGCTTGAACAG-3′.

Matrigel transwell invasion assay

Cells were serum starved overnight (0.1% DMEM), then 2×10^5 cells were seeded on top of 8 μm transwell inserts (BD Biosciences) with 0.1% DMEM and precoated with Matrigel (Becton, Dickinson and Company); 10% DMEM was used as a chemoattractant. After 24 hours, cells that had invaded through the Matrigel coated transwell inserts were fixed, stained by Kwik-Diff Stain (Thermo Fisher Scientific) and number of invading cells counted under ×10 using a Leica DM LB2 microscope (Leica Microsystems).

Published OnlineFirst October 21, 2013; DOI: 10.1158/0008-5472.CAN-13-1657

Soft agar assay

Cells were resuspended in DMEM containing 10% FBS, penicillin–streptomycin, and 0.22% (w/v) Agar-A (Bio Basic Inc.) and plated in triplicate on a base layer of 0.36% Agar-A (Bio Basic Inc.) in 6-well plates (12,000 cells/well), and placed in a humidified CO_2 incubator at 37°C. Twenty-five days later, colonies were counted.

Western blotting

Cells were lysed in ice-cold radioimmunoassay precipitation assay lysis buffer [50 mmol/L Tris pH 7.5, 150 mmol/L NaCl, 2 mmol/L EDTA pH 8.0, 0.5% (v/v) Triton X-100, and Complete protease inhibitor cocktail (Roche)]. Cell debris and insoluble material were removed by centrifugation at 12,000 × *g* at 4°C for 20 minutes. Following protein quantitation using the Bradford protein assay (Bio-Rad), 25 μg of lysate was loaded per lane and proteins resolved by 4% to 20% gradient SDS-PAGE gel, wet-transferred to polyvinylidene fluoride membranes (EMD Millipore), and the membranes were incubated in 5% nonfat dry milk in Tris-buffered saline Tween-20 (TBST; 10 mmol/L Tris-Base, 150 mmol/L NaCl, 0.05% Tween-20; pH 7.4) for 1 hour at room temperature to block nonspecific antibody binding, followed by incubation with primary antibody in 5% milk in TBST overnight at 4°C with gentle agitation. The membranes were washed 3 times for 10 minutes each in TBST, then incubated in TBST at room temperature for 1 hour, followed by three 10-minute washes with TBST. Protein–antibody binding on the membranes was detected with the use of enhanced chemiluminescence Plus solution (GE Healthcare Life Sciences) followed by exposure of the membranes to X-ray film (FujiFilm). The following primary antibodies were used: anti-phospho-Akt (Ser473), anti-Akt (pan) were from Cell Signaling Technology Inc., distributed by New England Biolabs. Anti-SGPP1 antibody was purchased from Abcam. Anti-β-actin antibody was purchased from Santa Cruz Biotechnology.

Luciferase assay

For SGPP1 3′UTR luciferase assays, PC3 or DU145 cells were transiently cotransfected with a SGPP1 3′UTR luciferase reporter plasmid or SGPP1 3′UTR luciferase reporter plasmid with mutations in the predicted miR-95 binding site (OriGene Technologies Inc.), pcDNA3 vector constitutively expressing *Renilla* luciferase, and miScript miRNA miR-95 mimic or miR control mimic. Twenty-four hours later, cells were processed for firefly luciferase and *Renilla* luciferase activity using the Dual Glo Luciferase Assay System. To normalize for transfection efficiency, the firefly luciferase activity was normalized to the *Renilla* luciferase activity. For miR-95 reporter luciferase assays, PC3 control or miR-95 stable cell lines were transfected with miR-95 target GoClone Reporter (SwitchGear Genomics), and 24 hours later processed for *Renilla* luciferase activity.

Fingolimod

Fingolimod (FTY720; Santa Cruz Biotechnology) was dissolved in ethanol, and cells were treated with vehicle (ethanol) or FTY720.

LY294002

LY294002 (Cell Signaling Technology) was dissolved in ethanol, and cells were treated with vehicle (ethanol) or LY294002.

Gene array expression

Total RNA was isolated from PC3 control and miR-95 stable cell lines using RNeasy Mini Kit (Qiagen) as per manufacturer's instructions, and gene expression profiling performed by The Centre for Applied Genomics (The Hospital for Sick Children, Toronto, Ontario, Canada) using an Affymetrix GeneChip Human Gene 2.0 ST array (Affymetrix). Gene expression array data were normalized using the default parameters in Affymetrix Expression Console Software (V.1.2). The expression data accession is GSE49559.

Tumor xenograft experiments

All experiments involving mice were performed according to University of Toronto and Sunnybrook Research Institute guidelines, using a peer-reviewed animal protocol. 2.5 million PC3-control, PC3-miR-95 cells, MDA-MB-231-control, and MDA-MB-231-miR-95 cells were mixed in a 1:1 (v:v) ratio with Growth Factor Reduced Matrigel (Becton, Dickinson and Company), and the mixture was injected subcutaneously into the right flanks of 6- to 7-week-old female athymic nude mice (Harlan). Tumor volume (in mm^3) was determined by caliper measurements performed every 3 to 4 days and calculated by using the modified ellipse formula (volume = length × $width^2/2$). When the xenograft tumor volumes reached approximately 150 mm^3, mice were randomly assigned to mock ionizing radiation or a 5 Gy dose of ionizing radiation delivered to the tumor, and tumor volumes determined every 3 to 4 days after ionizing radiation. Tumor growth delay was calculated by subtracting the average time for irradiated tumors to reach 3 times their starting volume from the average time of unirradiated tumors to reach 3 times their starting volume. When tumor volumes reached 3 times the starting volume, the mice were killed by cervical dislocation, and their tumors were excised, cut in half, with one half placed in Tissue-Tek O.C.T. compound (Fisher Scientific Co.) and stored at −80°C until cryosectioning and the remaining half flash frozen in liquid nitrogen.

Immunohistochemistry

Five-μm-thick tumor sections were stained with hematoxylin and eosin (H&E), and areas of necrosis delineated, quantitated, and expressed as a percentage of total tumor area (n = 3 tumors per group) as previously described (18). Sections were also immunostained for Ki-67, and the percentage of Ki-67 positive nuclei were quantitated from 6 representative fields (n = 3 tumors per group) as previously described (18). CD31 immunostaining for tumor vasculature was performed as previously described (18) and microvessel density (MVD) determined by finding tumor areas with the highest vascularity (hot spots) on low magnification (×5), and in each hot spot, CD31 positive microvessels were counted under high magnification (×20), with a positive microvessel defined as an endothelial cell or endothelial cell cluster that was clearly separated from adjacent microvessels, tumor cells, and other connective tissue elements.

Published OnlineFirst October 21, 2013; DOI: 10.1158/0008-5472.CAN-13-1657

miR-95 expression analysis in human prostate cancer patients

For TCGA prostate cancer analysis, miR data were retrieved from the Broad Institute Firehose website (https://confluence.broadinstitute.org/display/GDAC/Home; standardized data run: 2013_02_22) and analyzed using R. We previously described the patient characteristics and global miR profiling of our breast cancer patient dataset (19).

Statistical analysis

All statistical tests were 2-sided, and the statistical analysis was performed using the GraphPad Prism version 5.0 program (GraphPad Software). Statistical significance was defined as $P < 0.05$. The Student t test was used to compare the mean values between 2 groups. Data are presented as mean values with SDs unless otherwise noted.

Results

Radiation-resistant PC3 cancer cells possess an aggressive phenotype

To simulate the clinical scenario of radiation resistance, we treated PC3 prostate cancer cells with a course of daily fractionated ionizing radiation (mock or 2 Gy dose of ionizing radiation per day) over several weeks. Surviving cells were pooled and radiation clonogenic survival curves revealed that the surviving cells (PC3 rad res) were significantly more radiation resistant than the mock-irradiated control cells (PC3 parental; AUC PC3 rad res 1.78 vs. PC3 parental 1.49; $P < 0.05$; RPF = 1.19; Fig. 1A).

We further characterized the phenotype of PC3 rad res cells by assaying proliferation and cell-cycle profiles. PC3 rad res cells proliferated more quickly compared with parental cells both before [0 Gy: $6.0 \times 10^5 \pm 0.2$ cells (rad res) vs. $5.2 \times 10^5 \pm 0.4$ cells (parental); $P < 0.05$] and following ionizing radiation [6 Gy: $1.9 \times 10^5 \pm 0.1$ cells (rad res) vs. $1.3 \times 10^5 \pm 0.1$ cells (parental); $P < 0.01$; Fig. 1B]. Flow cytometric analysis revealed no significant differences between the PC3 rad res and PC3 parental cell cycle profiles before ionizing radiation [G_1 phase: $62.1 \pm 12.8\%$ (rad res) vs. $69.0 \pm 9.0\%$ (parental); S phase: $12.5 \pm 2.2\%$ (rad res) vs. $11.1 \pm .8\%$ (parental); G_2–M phase: $24.9 \pm 11.3\%$ (rad res) vs. $19.1 \pm 8.4\%$ (parental)]. In contrast, 24 hours following a 6 Gy dose of ionizing radiation, a significantly fewer percentage of PC3 rad res cells remained in the G_2–M phase compared with PC3 parental cells [$44.1 \pm 5.4\%$ (rad res) vs. $75.3 \pm 1.9\%$ (parental); $P < 0.01$], and correspondingly, a greater percentage of PC3 rad res cells were present in G_1 phase [$47.3 \pm 4.9\%$ (rad res) vs. $19.2 \pm 1.7\%$ (parental); $P < 0.01$; Fig. 1C]. This suggested that PC3 rad res were able to bypass the G_2–M checkpoint induced by ionizing radiation and continue progressing through the cell cycle.

The rad res cells were also cross-resistant to cisplatin [half maximal inhibitory concentration (IC_{50}) $19.5 \pm .7$ ng/mL (rad res) vs. IC_{50} $8.0 \pm .5$ ng/mL (parental); $P < 0.001$], which generates DNA DSBs (Fig. 1D) but not to docetaxel [IC_{50} 2.3 ± 1.0 ng/mL (rad res) vs. IC50 3.3 ± 2.0 ng/mL (parental)], which functions by preventing microtubule disassembly.

Invasiveness is an important property for an aggressive phenotype in cancer cells, which increases the propensity for regional lymphatic and distant metastatic spread, and may be enriched in radiation-resistant cancers (20). The Matrigel transwell invasion assay revealed that PC3 rad res cells invaded more readily than parental cells [$2.8 \pm .4$-fold (rad res) vs. 1.0-fold (parental); $P < 0.01$; Fig. 1E]. Consistent with a more aggressive phenotype, anchorage-independent growth was also significantly enhanced in PC3 rad res cells compared with parental cells [$1.4 \pm .1$ normalized colonies (rad res) vs. $1.0 \pm .1$ (parental) normalized colonies; $P < 0.05$; Fig. 1F]. Collectively, these results indicate that the PC3 rad res cells have acquired a more aggressive phenotype consisting of increased proliferation, impaired G_2–M cell-cycle arrest, and increased invasive potential.

miR-95 promotes radiation resistance and development of an aggressive phenotype

To identify candidate miRs involved in mediating radiation resistance, we performed next-generation sequencing on miRs isolated from PC3 rad res and parental cells. Because greater miR expression levels are known to correlate with higher target suppression and more robust regulatory capacity (21), we searched for candidates that had a high absolute expression (more than 100 reads per million, normalized counts). In this process, 8 candidate miRs were identified that were increased at least 2-fold in PC3 rad res cells compared with parental cells (Supplementary Table S1), including let-7e, whose family members have been demonstrated to be regulated by ionizing radiation, and can influence cellular radiation response (8, 22). We were interested in elucidating the function of miRs previously uncharacterized in radiation response, and thus assessed the function of a candidate miR, miR-95.

Using qRT-PCR, we confirmed that miR-95 expression was significantly increased in PC3 rad res cells compared with PC3 control cells by 1.9-fold [$1.9 \pm .2$ (rad res) vs. 1.0 (control); $P < 0.01$; Fig. 2A], which was in close agreement with the fold change seen from the next-generation sequencing data. miR-95 expression was significantly upregulated 1.7-fold within 0.5 hours following ionizing radiation in PC3 cells [$1.7 \pm .1$ (0.5 hour) vs. 1.0 (0 hour); $P < 0.01$], and then returned to baseline by 2 hours, indicating that miR-95 is acutely upregulated by ionizing radiation (Fig. 2B).

PC3 cells were transiently transfected with a miR-95 mimic or a control mimic and radiation clonogenic survival assays performed. The miR-95 mimic-transfected PC3 cells displayed significantly increased radiation resistance compared with control cells [AUC 1.74 (miR-95) vs. 1.35 (control); $P < 0.05$; RPF = 1.28; Fig. 2C]. Transfection of a miR-95 mimic was also able to induce radiation resistance in additional carcinoma cells and a nonmalignant cell line: DU145 prostate carcinoma cells [AUC 2.16 (miR-95) vs. 1.83 (control); $P < 0.05$; RPF = 1.18], MDA-MB-231 breast carcinoma cells [AUC 2.06 (miR-95) vs. 1.82 (control); $P < 0.05$; RPF = 1.13], and MCF10A normal breast epithelial cells [AUC 1.77 (miR-95) vs. 1.48 (control); $P < 0.05$; RPF = 1.19; Fig. 2A]. We assayed the influence of another candidate, miR-320a, on radiation survival in PC3 cells, but did not observe any change (data not shown).

To further investigate the function of miR-95 in radiation resistance and aggression, we transduced PC3 cells with a

Published OnlineFirst October 21, 2013; DOI: 10.1158/0008-5472.CAN-13-1657

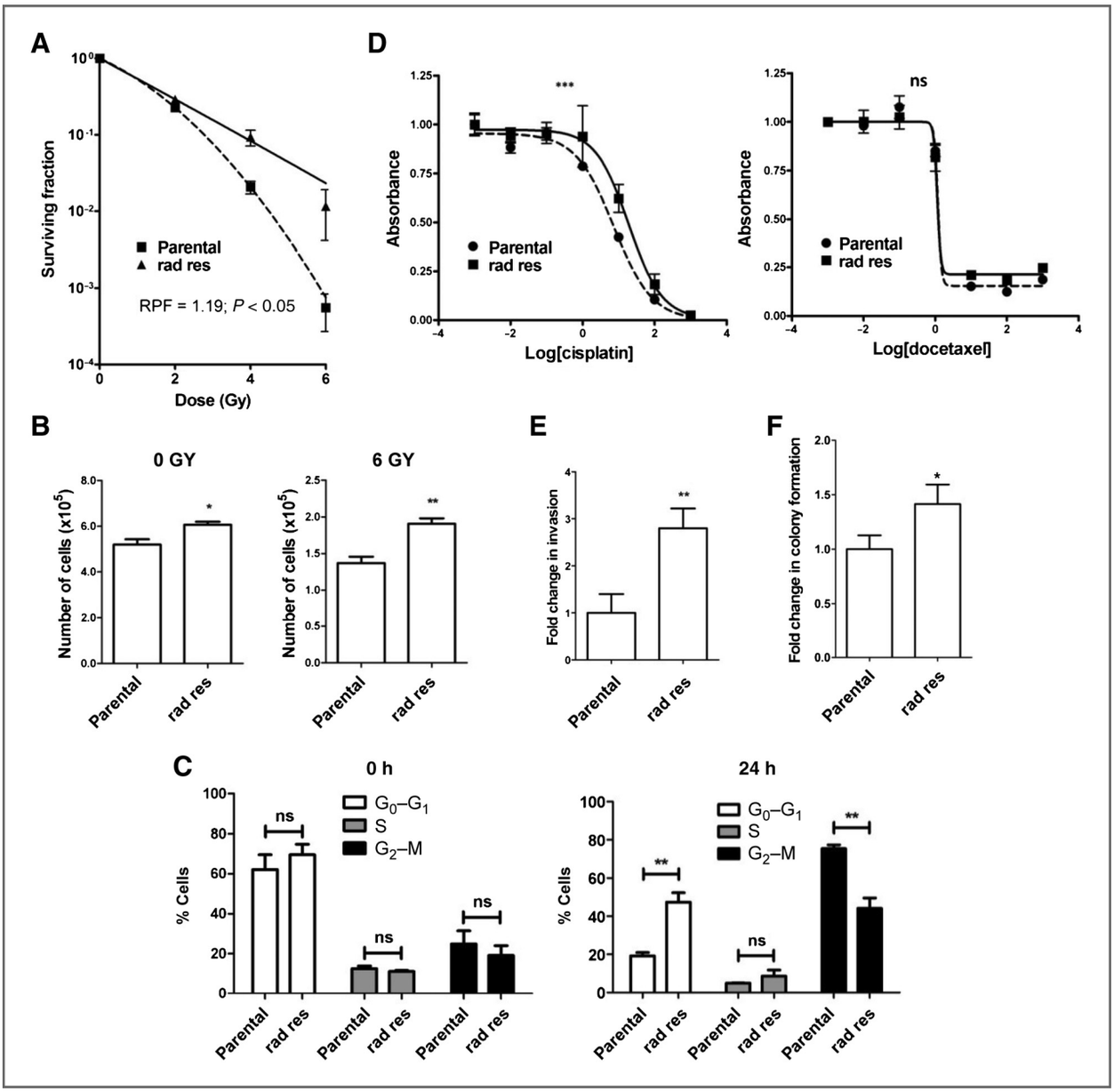

Figure 1. PC3 cells surviving radiation treatment are radiation resistant and have an aggressive phenotype characterized by increased proliferation, invasive potential, and impaired G_2–M cell cycle arrest. A, PC3 cells were mock irradiated with 0 Gy (PC3 parental) or irradiated with a total of 2 Gy × 45 daily fractions of ionizing radiation (PC3 rad res), radiation clonogenic survival assays performed, and surviving fraction fitted to the linear-quadratic equation. B, cell counts of viable PC3 parental and rad res cells following mock ionizing radiation (0 Gy) or 6 Gy dose of ionizing radiation. C, cell-cycle profiles of PC3 parental and rad res cells following a 6 Gy dose of ionizing radiation at 0 or 24 h. D, cell viability assay of PC3 parental and rad res cells treated with increasing concentrations of cisplatin and docetaxel (ng/mL) shown in log scale. E, Matrigel transwell invasion assay of PC3 parental and rad res cells. F, soft agar assay of PC3 parental and rad res cells. Means, SDs, and statistical significance are denoted; *, $P < 0.05$, **, $P < 0.01$, ***, $P < 0.001$; ns, nonsignificant difference; $n = 3$ independent experiments.

lentivirus harboring miR-95 (PC3-miR-95) or the control sequence (PC3-control) to generate stable cell lines following antibiotic selection. We verified increased miR-95 activity in PC3-miR-95 cells relative to PC3-control cells through the use of a miR-95 luciferase reporter vector (Supplementary Fig. S1). We also verified that PC3-miR-95 cells were more radiation resistant than PC3-control cells, similar to the results obtained with the miR-95 mimic experiments (data not shown). PC3-miR-95 cells proliferated significantly quicker than PC3-control cells before [$6.2 \times 10^5 \pm 0.4 \times 10^5$ cells (miR-95) vs. $4.3 \times 10^5 \pm 0.3 \times 10^5$ cells (control); $P < 0.001$] and following a 6 Gy dose of ionizing radiation [$1.9 \times 10^5 \pm 0.2 \times 10^5$ cells (miR-95) vs. $1.2 \times 10^5 \pm 0.3 \times 10^5$ cells (control); $P < 0.05$; Fig. 3A]. Flow cytometric analysis revealed no significant differences in cell-

Published OnlineFirst October 21, 2013; DOI: 10.1158/0008-5472.CAN-13-1657

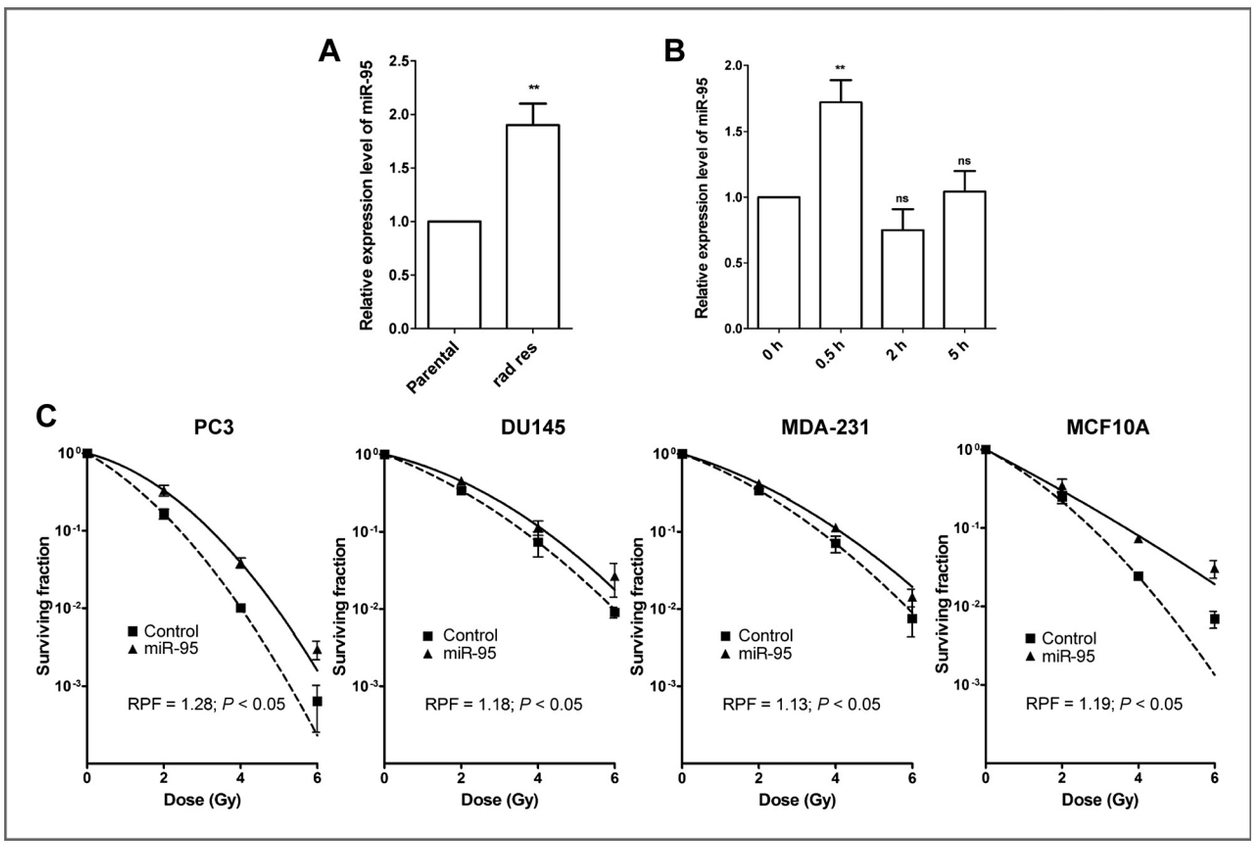

Figure 2. miR-95 expression is elevated in radiation-resistant cells and increases survival following irradiation. A, qRT-PCR was performed using miR-95–specific primers to determine relative endogenous expression levels of miR-95 in PC3 parental and rad res cells. B, PC3 parental cells at 0, 0.5, 2, and 5 hours following a 6 Gy dose of ionizing radiation (expression was normalized to SNORD61). C, radiation clonogenic survival assays were performed, and surviving fraction fitted to the linear quadratic equation for PC3, DU145, MDA-231, and MCF10A cells transiently transfected with control or miR-95 mimic. Means, SDs, and statistical significance are denoted; **, $P < 0.01$; ns, nonsignificant difference; $n = 3$ independent experiments.

cycle profiles between PC3-miR-95 and PC3-control cells before irradiation [G_1 phase: 42.6% ± 3.3% (miR-95) vs. 41.8 ± 1.9% (control); S phase: 9.8 ± 3.2% (miR-95) vs. 8.7 ± 2.2% (control); G_2–M phase: 47.5 ± 6.1% (miR-95) vs. 49.4 ± 4.3% (control)], however 24 hours following 6 Gy ionizing radiation, there was a smaller percentage of PC3-miR-95 cells in the G_2–M phase compared with PC3-control cells [53.0 ± 2.1% (miR-95) vs. 59.6 ± 1.3% (control); $P < 0.05$; Fig. 3B]. These results suggest that miR-95 mimic-transfected PC3 cells were able to partly overcome an ionizing radiation–induced block at G_2–M phase, and continue through the cell cycle. Moreover, given that replicative senescence is a major form of cell death after ionizing radiation, we quantified senescent cells via cytochemical detection of senescence-associated (SA)-β-galactosidase. Following ionizing radiation, there were fewer senescent PC3-miR-95 cells compared with PC3-control cells [29.7 ± 9.1% (miR-95) vs. 47.6 ± 9.0% (control); $P < 0.01$; Fig. 3C], indicating that miR-95 can reduce radiation-induced cell death by affecting senescence. Very few senescent cells were seen in nonirradiated PC3-miR-95 and PC3-control 95 cells, although there was a significant difference noted [0.2 ± 0.1% (miR-95) vs. 0.6 ± 0.3% (control); $P < 0.05$; data not shown].

In keeping with an aggressive phenotype, PC3-miR-95 cells also possessed increased invasiveness [3.0 ± .2-fold (miR-95) vs. 1.0-fold (control); $P < 0.01$; Fig. 3D] and increased anchorage-independent growth [1.9 ± .2-fold (miR-95) vs. 1.0-fold; $P < 0.01$; Fig. 3E). To explore the mechanisms of miR-95 action further downstream, we determined the level of activated Akt in these cells because the PI3K-Akt pathway is known to regulate radiation sensitivity (23). Indeed, Western blotting analysis of PC3-control and PC3-miR-95 cells mock irradiated or irradiated with a 6 Gy dose of ionizing radiation revealed increased Akt activation in PC3-miR-95 cells (Fig. 3F). Similar results were seen in DU145 cells, where transient transfection of miR-95 mimic promoted increased proliferation prior to [$4.4 \times 10^5 \pm 0.6 \times 10^5$ cells (miR-95) vs. $2.0 \times 10^5 \pm 0.2 \times 10^5$ cells (control); $P < 0.001$] and 24 hours following a 6 Gy dose of ionizing radiation [$2.5 \times 10^5 \pm 0.1 \times 10^5$ cells (miR-95) vs. $1.8 \times 10^5 \pm 0.3 \times 10^5$ cells (control); $P < 0.05$], disrupted G_2–M cell-cycle arrest following ionizing radiation [G_1 phase: 54.1% ± 6.5% (miR-95) vs. 71.5 ± 2.2% (control), $P < 0.05$; S phase: 5.7 ± 1.4% (miR-95) vs. 5.5 ± 1.9% (control); G_2–M phase: 40.1 ± 5.2% (miR-95) vs. 23.0 ± 1.8% (control), $P < 0.01$], enhanced invasion [2.8 ± 1.1-fold (miR-95) vs. 1.0-fold (control); $P < 0.05$], and increased phospho-AKT (Supplementary Fig. S2). Together,

Published OnlineFirst October 21, 2013; DOI: 10.1158/0008-5472.CAN-13-1657

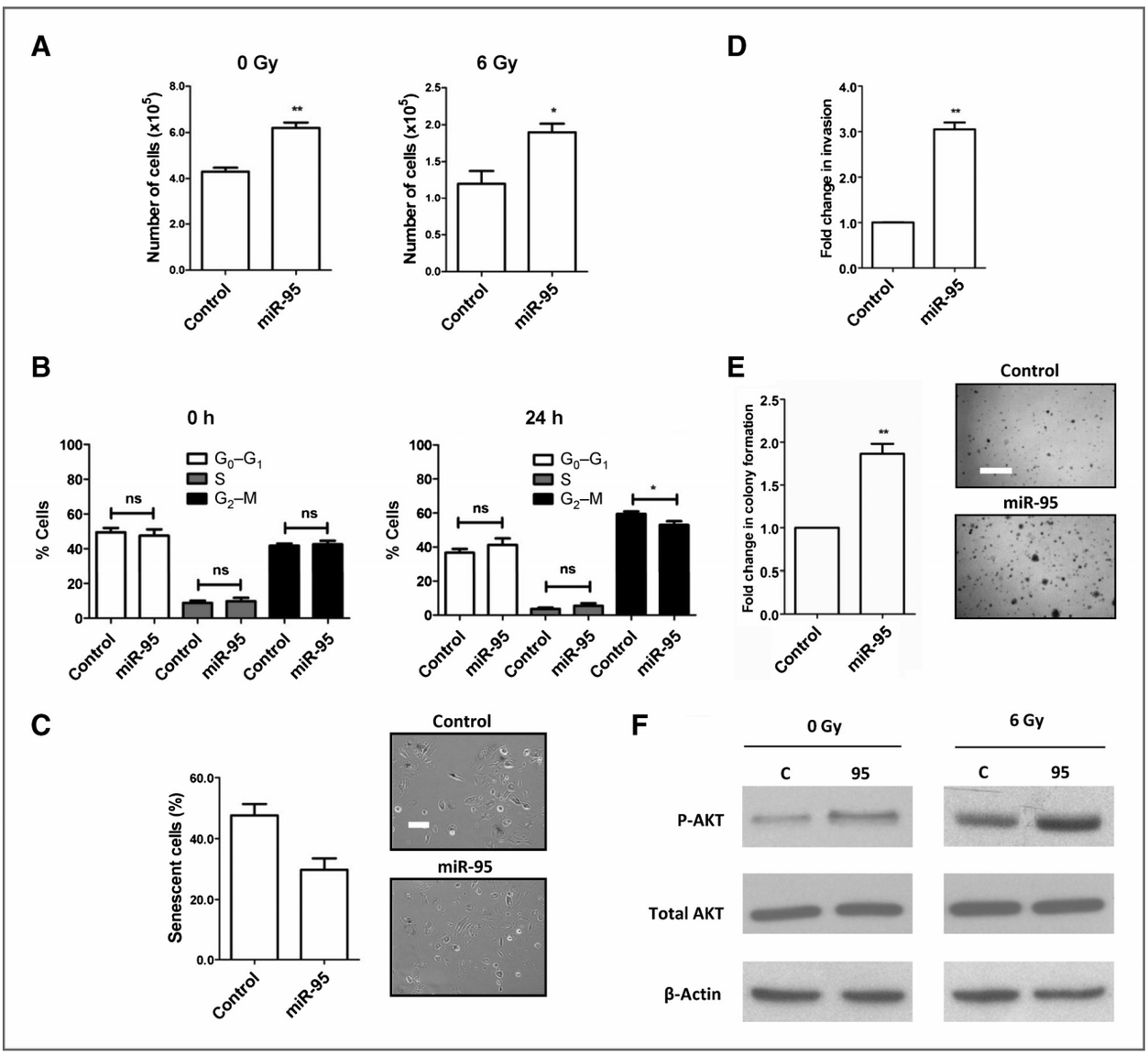

Figure 3. miR-95 promotes an aggressive phenotype. A, proliferation of PC3-control and PC3-miR-95 cells at 4 days after mock ionizing radiation (IR; 0 Gy) or 6 Gy IR. B, cell-cycle profiles of PC3-control and PC3 miR-95 cells at 0 and 24 h following 6 Gy IR. C, β-galactosidase senescence assay of PC3-control and PC3-miR95 cells following a 6 Gy dose of IR (scale bar, 200 μm). D, Matrigel invasion assay of PC3-control and PC3-miR-95 cells. E, soft agar assay of PC3-control and PC3-miR-95 cells with representative images (scale bar, 300 μm). F, Western blotting for phospho-AKT (P-AKT), total AKT, and β-actin (loading control) from PC3-control (C) and PC3-miR-95 (95) cells at 24 h after mock IR or 6 Gy IR; representative experiment shown. Means, SDs, and statistical significance are denoted; *, $P < 0.05$, **, $P < 0.01$; ns, nonsignificant difference; $n = 3$ independent experiments.

these findings indicate that miR-95 is associated with an aggressive phenotype through numerous potential mechanisms, including radiation resistance, similar to that observed in radiation-resistant cells.

miR-95 promotes radiation resistance through downregulation of SGPP1

To identify targets of miR-95 responsible for its cellular phenotype, we used a dual-pronged approach of *in silico* target prediction using Targetscan Human release 6.0 (24) in combination with microarray expression profiling generated from PC3-miR-95 vs. PC3-control cells (Supplementary Table S2). This strategy identified 28 overlapping targets, of which four overlapping candidate gene targets (*DICER1*, *UBE4B*, *SGPP1*, and PTPN21) were further analyzed based upon their potential involvement in radiation resistance or oncogenic processes (11, 25–28). Using qRT-PCR, we verified that their expression were significantly decreased in PC3-miR-95 cells relative to PC3-control cells (Fig. 4A). Of these candidates, we selected SGPP1 for further study, because SGPP1 catalyzes the conversion of the prosurvival sphingolipid, sphingosine-1-phosphate (S1P), to sphingosine that can promote cell death (29).

Published OnlineFirst October 21, 2013; DOI: 10.1158/0008-5472.CAN-13-1657

Western blotting confirmed decreased protein expression of SGPP1 in PC3-miR-95 cells relative to PC3-control cells (Fig. 4A). Downregulation of SGPP1 was also seen in DU145 cells transfected with a miR-95 mimic compared with a control mimic (Supplementary Fig. S3). To assess the candidacy of the SGPP1 3′UTR region as a target of miR-95, we used the Targetscan miR target prediction program that identified one putative miR-95 binding site in the 3′UTR of SGPP1 (Fig. 4B). We cotransfected a luciferase reporter plasmid bearing the 3′UTR of SGPP1 into PC3 cells with control or miR-95 mimic. Our results revealed a significant reduction in luciferase activity in PC3 miR-95 transfected cells compared with control mimic transfected cells [0.71 ± 0.08 luciferase activity (miR-95) vs. 1.0 luciferase activity (control); $P < 0.001$; Fig. 4B]. Furthermore, mutation of the predicted miR-95 binding site in the SGPP1 3′ UTR reconstituted luciferase activity [0.98 ± 0.06 luciferase activity (miR-95) vs. 1.0 luciferase activity (control)], thus validating SGPP1 as a bona-fide target of miR-95 (Fig. 4B). We noted similar findings in DU145 cells, with miR-95 expression mediating significant downregulation of wild-type SGPP1 3′UTR luciferase activity [wild-type 3′UTR: 0.42 ± 0.05 luciferase activity (miR-95) vs. 1.0 luciferase activity (control), $P < 0.01$], but not mutant SGPP1 3′UTR luciferase activity [mutant 3′UTR: 0.91 ± 0.08 luciferase activity (miR-95) vs. 1.0 luciferase activity (control)].

Because previous studies have demonstrated that SGPP1 activity can result in decreased S1P levels (27, 30), and S1P has been reported to activate the Akt pathway and protect cells

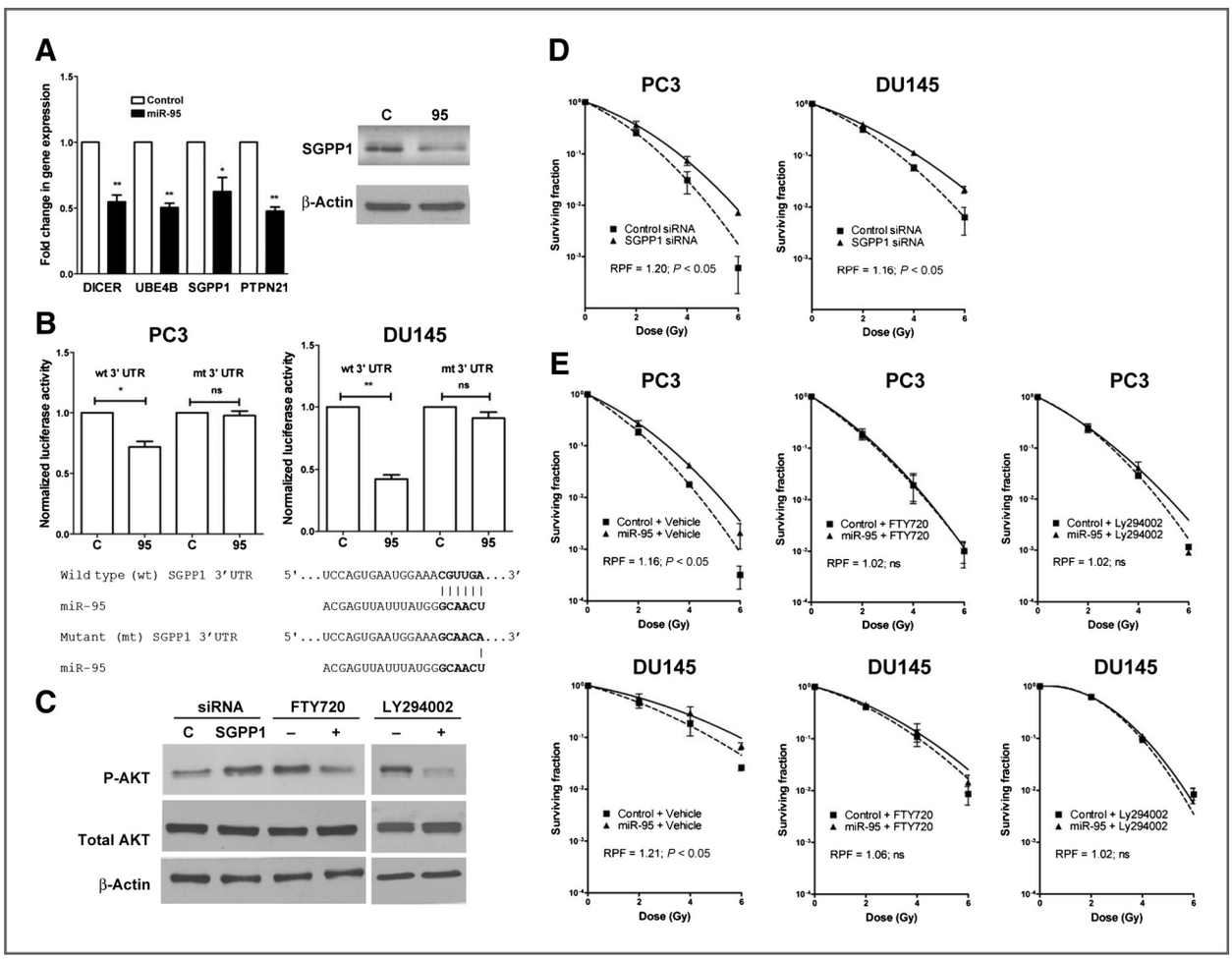

Figure 4. SGPP1 is a target of miR-95 and promotes radiation resistance. A, relative expression levels of DICER1, UBE4B, SGPP1, and PTPN21 in PC3-control and PC3-miR-95 cells determined via qRT-PCR. Representative Western blot for SGPP1 and β-actin are shown. B, wild type (wt) or mutant (mt) 3′UTR-SGPP1 firefly luciferase reporter vector was transiently cotransfected into PC3 and DU145 cells with *Renilla* luciferase vector, and control (C) or miR-95 (95) mimic, and firefly luciferase activity normalized to *Renilla* luciferase activity. The predicted miR-95 binding site in the wt SGPP1 UTR and mt SGPP1 UTR is shown. C, Western blot for phospho-AKT (P-AKT), total AKT, and β-actin levels in PC3 cells transiently transfected with SGPP1 siRNA or control siRNA (C), or treated with FTY720, LY294002, or vehicle (–). D, radiation clonogenic survival assays were performed following siRNA-mediated knockdown of SGPP1 in PC3 and DU145 cells, and surviving fraction fitted to the linear quadratic equation. E, radiation clonogenic survival assays were performed in PC3-control and PC3-miR-95 cells or DU145 cells transiently transfected with control or miR-95 mimic, treated with vehicle, FTY720 or LY294002, and surviving fraction fitted to the linear quadratic equation. Means, SDs, and statistical significance are denoted; *, $P < 0.05$, **, $P < 0.01$; ns, nonsignificant difference; $n = 3$ independent experiments.

Published OnlineFirst October 21, 2013; DOI: 10.1158/0008-5472.CAN-13-1657

from ionizing radiation–induced cell death (31), we performed siRNA-mediated knockdown of SGPP1 (Supplementary Fig. S4). Consistent with this, we observed that siRNA-mediated SGPP1 knockdown increased phospho-AKT levels in PC3 cells (Fig. 4C), whereas treatment with FTY720, a small molecule inhibitor of S1P signaling, decreased phospho-AKT levels (Fig. 4C); phospho-AKT levels were also potently inhibited with the phosphatidylinositol 3 kinase (PI3K) inhibitor, LY294002. We also assessed the functional consequences of a reduction in SGPP1 expression, and noted that SGPP1 knockdown conferred increased radiation resistance in PC3 cells [AUC PC3 SGPP1 siRNA 1.89 vs. AUC PC3 control 1.57, $P < 0.05$; RPF = 1.20) and DU145 cells (AUC DU145 SGPP1 siRNA 2.04 vs. AUC DU145 control 1.75, $P < 0.05$; RPF = 1.16; Fig. 4D], phenocopying that seen in miR-95-overexpressing cells. siRNA-mediated knockdown of the other 3 candidate gene targets (*DICER1*, *UBE4B*, *PTPN21*) did not influence radiation survival in PC3 cells (data not shown). Interestingly, FTY720 treatment abrogated the radiation resistance of PC3-miR-95 cells (AUC PC3 miR-95 + FTY720 1.43 vs. AUC PC3 control + FTY720 1.40; RPF = 1.02) and DU145 cells transfected with miR-95 [AUC DU145 miR-95 + FTY720 2.19 vs. AUC DU145 control + FTY720 2.05; RPF = 1.06; Fig. 4E], supporting the importance of S1P signaling in miR-95 promotion of radiation resistance. Inhibition of the PI3-K-Akt pathway with LY294002 also abrogated the radiation resistance of PC3-miR-95 cells and DU145 miR-95 cells (AUC PC3 miR-95 + LY294002 1.59 vs. AUC PC3 control + LY294002 1.55; RPF = 1.02) and DU145 cells transfected with miR-95 (AUC DU145 miR-95 + LY294002 2.48 vs. AUC DU145 control + LY294002 2.44; RPF = 1.02). Taken together, our results strongly suggest that miR-95 targets SGPP1, activating the PI3-K-AKT pathway, which renders cancer cells more resistant to radiation treatment.

miR-95 promotes tumor growth and radiation resistance *in vivo*

To model the *in vivo* consequences of miR-95 overexpression in tumors on growth rates and radiation response, we generated subcutaneous tumors in athymic nude mice using PC3-control and PC3-miR-95 cells, followed by irradiation of the tumors with a 5 Gy dose of ionizing radiation or mock ionizing radiation (Fig. 5A). The mock-irradiated PC3-miR-95 tumors

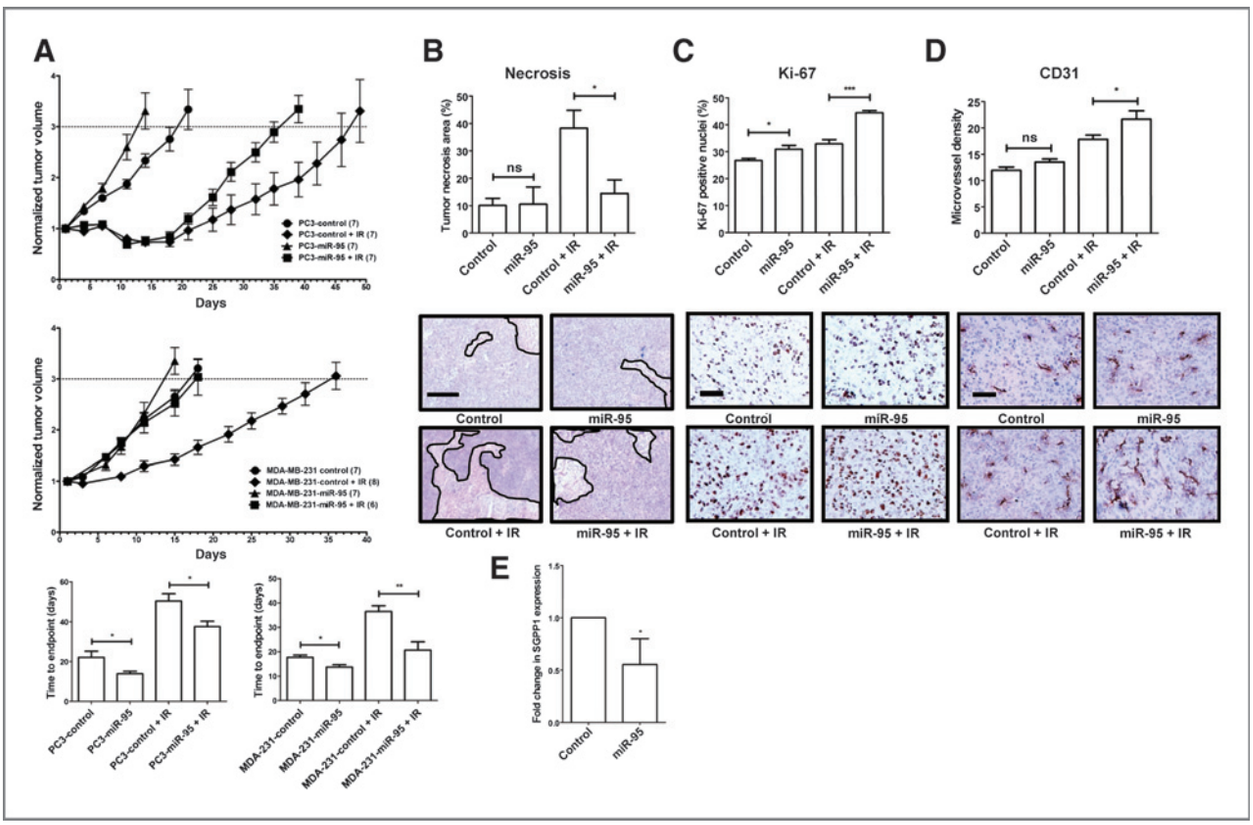

Figure 5. miR-95 increases tumorigenicity and radiation resistance *in vivo*. A, PC3 and MDA-MB-231 control and miR-95 tumors were treated with mock ionizing radiation (IR; 0 Gy) or 5 Gy dose of IR on day 1. Dotted line, endpoint of 3 times starting volume. Mean tumor volumes normalized to starting volume and SEMs are denoted with number of mice in each group shown in parentheses. Time to reach endpoint is shown with means and SEM with statistical significance denoted. B, H&E staining of PC3-control and miR-95 tumors with areas of necrosis quantitated and representative images shown with regions of necrosis outlined (scale bar, 500 μm). C, anti-Ki-67 immunostaining of PC3-control and miR-95 tumors (scale bar, 100 μm) with percentage of Ki-67 positive nuclei plotted above. D, anti-CD31 immunostaining of PC3-control and miR-95 tumors to identify tumor vasculature (scale bar, 100 μm), and microvessel density plotted above. E, qRT-PCR of SGPP1 in PC3-miR95 and PC3-control tumors ($n = 3$ per group). Means, SDs, and statistical significance are denoted; *, $P < 0.05$, **, $P < 0.01$, ***, $P < 0.001$; ns, nonsignificant difference.

Published OnlineFirst October 21, 2013; DOI: 10.1158/0008-5472.CAN-13-1657

grew more quickly than the PC3-control tumors [time to reach 3 times starting volume 13.8 ± 3.3 days (miR-95) vs. 22.0 ± 8.1 days (control)], and were more radiation resistant as demonstrated by a shorter growth delay [23.6 days (miR-95) vs. 28.2 days (control)].

Upon reaching 3 times the size of the initial volume, tumors were removed and H&E staining was performed to identify regions of tumor necrosis. Significantly less necrosis was noted in PC3-miR-95 tumors compared with PC3-control tumors following ionizing radiation [14.4 ± 4.9% (miR-95) vs. 38.2 ± 6.5% (control); $P < 0.05$], however no difference in necrosis was identified in unirradiated tumors [10.5 ± 6.2% (miR-95) vs. 10.0 ± 2.6% (control); $P < 0.05$; Fig. 5B]. Moreover, immunostaining for the proliferative marker, Ki-67, indicated that more proliferative cells were present in the PC3-miR-95 tumors relative to PC3-control tumors [30.8 ± 1.4% (miR-95) vs. 26.7 ± 0.7% (control); $P < 0.05$], particularly in irradiated tumors [44.4 ± 0.84% (miR-95) vs. 32.8 ± 1.5% (control); $P < 0.01$; Fig. 5C]. Anti-CD31 immunostaining followed by MVD determination revealed that MVD was significantly increased in the PC3-miR-95 tumors compared with the PC3-control tumors following irradiation [21.6 ± 1.5 (miR-95) vs. 17.8 ± 0.7 (control); $P < 0.05$], although no significant difference was noted in unirradiated tumors [13.5 ± 0.6 (miR-95) vs. 11.9 ± 0.6 (control); Fig. 5D]. Together, the histological data provide support to our observations that miR-95 overexpression in PC3 tumors promotes radiation resistance *in vivo*. Notably, our qRT-PCR analysis showed that SGPP1 expression remained reduced in PC3 miR-95 tumor xenografts relative to control xenografts [0.55 ± 0.24-fold (miR-95) vs. 1.0-fold (control); $P < 0.05$], thus supporting our *in vitro* findings (Fig. 5E).

To confirm our *in vivo* findings in an additional tumor type, we repeated tumor xenograft experiments using MDA-MB-231 cells stably overexpressing control mimic (MDA-MB-231-control) or miR-95 mimic (MDA-MB-231-miR-95; Fig. 5A). The MDA-MB-231-miR-95 tumors grew quicker than control tumors [time to reach 3 times starting volume 13.7 ± 2.5 days (miR-95) vs. 17.7 ± 2.5 days (control)] and were considerably more radiation resistant as evidenced by the shorter growth delay [6.9 days (miR-95) vs. 18.8 days (control)].

miR-95 expression is increased in human prostate and breast cancer

To further support our findings that miR-95 promotes a range of tumorigenic processes, we proceeded to data mine The Cancer Genome Atlas (TCGA), and found that miR-95 is significantly elevated ($P < 0.0001$) in primary prostate cancer patient specimens compared with normal prostate controls (Fig. 6A). The association between miR-95 expression and biochemical-free relapse survival (BFRS) was analyzed using the Cox proportional hazard regression model; miR-95 expression was positively associated with risk of BFRS in this patient cohort ($P = 0.014$; HR = 2.2; 95% CI, 1.2–4.1). When patients were dichotomized into high (≥ median) and low (< median) miR-95 expression, and the log-rank test was performed to compare risk of BFRS in high-expression versus low-expression groups, there was also a trend toward increased risk of BFRS in patients with high miR-95 expression, however this did not reach statistical significance ($P = 0.13$; Fig. 6A). Although follow-up is relatively modest (median = 1.2 years) and there are only 8 cases of biochemical relapse recorded in this TCGA dataset, these results provide compelling evidence for further investigation into the role of miR-95 as a predictor of relapse in prostate cancer patients. In a previous study, we had performed global miR profiling of 71 lymph-node negative breast cancer patients, and 5 normal controls (19, 32). With this study, we now provide new evidence that miR-95 is significantly elevated in breast cancer patients compared with normal controls ($P < 0.01$; Fig. 6B). There was a trend toward higher miR-95 expression level in breast cancer patients who experienced a recurrence relative to those patients who did not, however this did not reach statistical significance ($P = 0.16$). Collectively, these clinical data demonstrate for the first time, miR-95 is overexpressed in human prostate and breast cancer patients.

Discussion

Tumor resistance to radiation treatment remains a clinical problem, and research addressing this challenging problem is essential. We believe that researching the role of miRs in radiation resistance is a promising avenue given their ability to regulate multiple oncogenic processes including response to therapy. To address this problem, we generated a radiation-resistant cancer cell model, and discovered that it displays an aggressive phenotype typically seen in the clinical scenario of recurrent tumors. Next-generation sequencing identified a number of miRs enriched in these radiation-resistant cells, and one of these candidates, miR-95 was the focus of this research. To gain insight into miR-95 function, we performed *in vitro* experiments and human xenograft studies, and demonstrated that miR-95 regulates a range of cellular processes that can promote tumor progression including proliferation, invasion, anchorage-independent growth, and resistance to ionizing radiation. The involvement of miR-95 in mediating these pleotropic processes highlights its oncogenic potential. These findings are clinically relevant, given our discovery that miR-95 is significantly upregulated in human prostate and breast cancer specimens, as well as previous reports indicating that miR-95 expression is upregulated in human colorectal and pancreatic carcinoma samples compared with normal controls (15, 16). miR-95 overexpression may play an important role in tumorigenesis in a multiple cancer types and adversely influence their response to radiotherapy.

Our study provides novel insight into miR-95 function in increasing clonogenic survival following ionizing radiation in prostate and breast cancer cells, in addition to nontransformed normal breast epithelial cells, indicating that this effect is conserved between different cell types. In addition, the cells tested in our ionizing radiation clonogenic studies varied with regards to p53 status (PC3: null p53, DU145: mutant p53, MDA-MB-231: mutant p53, MCF10A: wild-type p53), and thus, miR-95 seems to promote radiation resistance independent of p53 function. We have begun exploring the mechanistic basis of miR-95 action, which seems to lie in the regulation of the S1P-PI3K-Akt pathway. Engagement of the PI3K-Akt pathway is a major determinant of survival

Published OnlineFirst October 21, 2013; DOI: 10.1158/0008-5472.CAN-13-1657

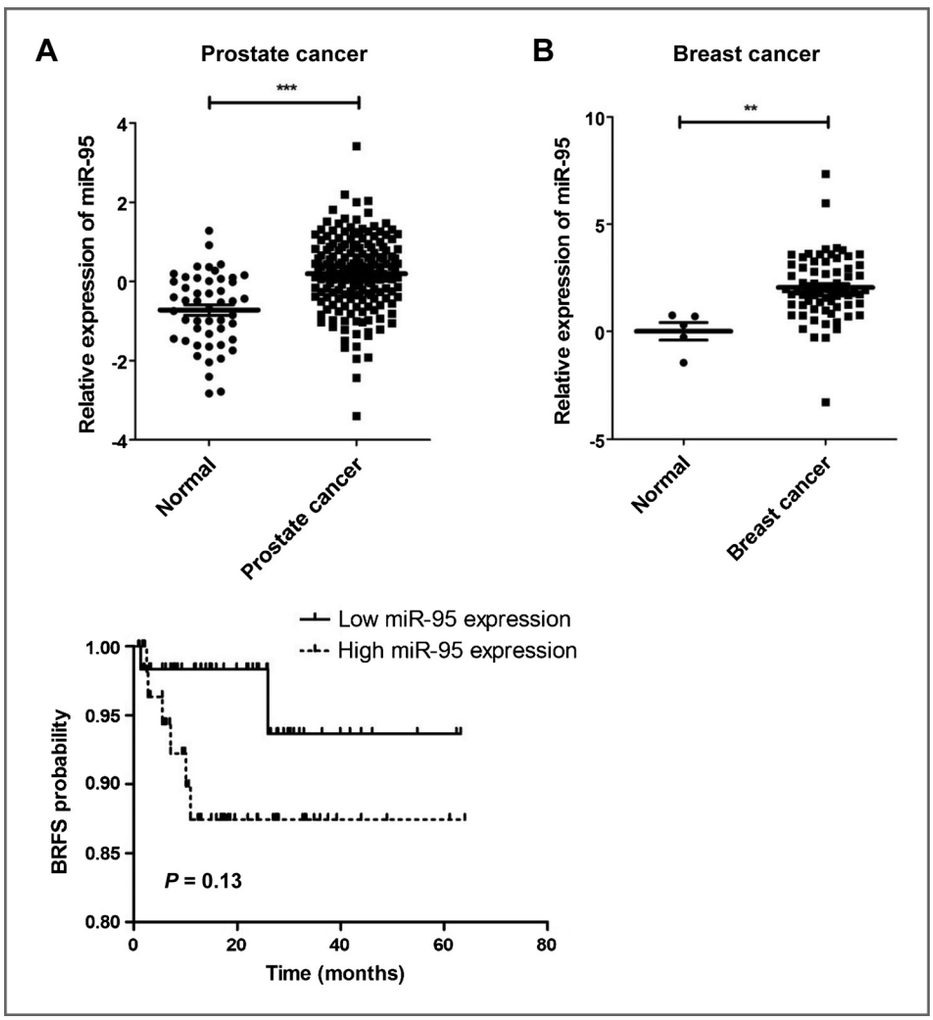

Figure 6. miR-95 expression is increased in human prostate and breast cancer. A, database mining of TCGA prostate cancer database indicated increased miR-95 expression in prostate cancer samples compared with normal prostate controls. The association between miR-95 expression and BFRS was analyzed using the Cox proportional hazard regression model and also dichotomized into high (≥ median) and low (< median) miR-95 expression (shown). B, global miR profiling revealed increased miR-95 expression in breast cancer patients compared with normal controls. Expression is represented as $\log_2$ transformed data; **, $P < 0.01$, ***, $P < 0.0001$.

after radiation (23). S1P is a highly bioactive sphingolipid known to activate Akt and protect against ionizing radiation–induced cell death (31). S1P can be generated by phosphorylation of sphingosine by sphingosine kinase 1 (SK1), whereas S1P dephosphorylation by SGPP1 produces sphingosine, which is known to promote cell death (27). We have identified SGPP1 as a novel direct target of miR-95, whereby SGPP1 downregulation by miR-95 increased AKT activation, and increased cancer cell survival following radiation treatment.

Although we do not address the S1P levels in miR-95–overexpressing cancer cells directly, our observations about radiation resistance in miR-95–overexpressing cancer cells are likely explained through an increase in S1P mediated by the suppression of SGPP1 expression, which has been shown to protect against radiation-induced cell death (31). Indeed, the regulation of SGPP1 and hence S1P/sphingosine balance by miR-95 highlights the potential importance of this miR, because S1P can act as an intracellular second messenger, or bind to S1P receptors (G-protein–linked receptors), and thus regulate diverse cancer processes including migration, invasion, cell death, and angiogenesis (reviewed in ref. 29). Our model of miR-95 action in S1P regulation is further supported by the fact that treatment of miR-95–overexpressing cells with the S1P signaling inhibitor FTY720 specifically sensitized these cells to radiation treatment. Interestingly, the ionizing radiation clonogenic survival curve of PC3-miR-95 cells treated with FTY720 overlapped the survival curve of PC3-control cells, suggesting that S1P signaling may be a major source of radiation resistance in miR-95-overexpressing cells (31). Another study also reported that siRNA-mediated knockdown of SGPP1 expression in breast cancer cells results in increased S1P levels, with a concomitant increase in resistance to cell death following TNF-α and daunorubicin treatment (27). In addition, Nava and colleagues showed that treatment of LNCaP prostate cancer cells with either a sphingosine kinase inhibitor or exogenous sphingosine, which act to decrease the ratio of S1P to sphingosine, resulted in sensitization of LNCaP prostate cancer cells to radiation-induced cell death (33). Furthermore, Brizuela and colleagues have recently reported that knockdown of sphingosine-1-phosphate lyase (another phosphatase that acts to decrease S1P levels) decreased

Published OnlineFirst October 21, 2013; DOI: 10.1158/0008-5472.CAN-13-1657

γ-H2AX foci following irradiation in prostate cancer cells (34). Collectively, the findings presented in this study, as well as the other reports support a model where miR-95 targeting of SGPP1 leads to an increase in cellular S1P levels, with subsequent activation of the PI3K-Akt pathway, resulting in cell survival and proliferation (Fig. 7).

This highlights the exciting possibility of sensitizing miR-95–overexpressing tumors to ionizing radiation by targeting the S1P pathway. Clinical data support the importance of the S1P pathway in cancer outcomes, as increased expression of SK1 is seen in a range of tumor types including prostate and breast cancer, and is associated with poor patient outcomes (reviewed in ref. 29). Helleman and colleagues generated a 9-gene set to predict cisplatin resistance in ovarian cancer patients, and underexpression of SGPP1 is one of the 9 genes that predicts for cisplatin resistance (35). It is interesting to speculate whether miR-95 overexpression could be a mechanism for decreased SGPP1 in these patients, and result in increased cellular S1P and resistance to cisplatin. In ionizing radiation and chemotherapy cancer resistance, the S1P pathway is emerging as an important therapeutic target. Fingolimod (FTY720), an orally active sphingosine inhibitory analogue that we have utilized, was developed to target this pathway, and has recently been approved for use in multiple sclerosis patients to reduce the rate of relapses, presumably by preventing lymphocyte egress from lymphoid organs (36, 37). The potential clinical utility of FTY720 is not limited to multiple sclerosis; Pchetski and colleagues previously demonstrated that FTY720 radiosensitizes PC3 and DU145 prostate cancer cells (38). Although our results seem to be at odds with their report, because we only observed radiosensitization of PC3-miR-95 overexpressing cells and not PC3-control cells, this discrepancy may be because of the lower concentration of FTY720 used in our study (0.5 μmol/L) compared with their study (1 μmol/L). The basis of the lower concentration of FTY720 that we selected for our study lies in the excessively high reduction in clonogenic survival (>0.5) seen with FTY720 concentrations of 1 μmol/L or higher (Supplementary Fig. S5). Moreover, our endpoints differed in that, Pchejetski's study used the endpoint of cell viability as opposed to clonogenic survival, for assessing radiosensitivity. FTY720 and other novel inhibitors of the S1P pathway are being investigated preclinically as anticancer therapy (reviewed in ref. 29), and we postulate that they may prove to be clinically useful for radiosensitizing tumors that overexpress miR-95. Blockade of S1P signaling by FTY720 seems to be well tolerated in humans when administered in the short term (29). Thus, FTY720 may seem to be a promising agent to consider for tumor radiosensitization in patients. However, it is important to first consider that FTY720 may also influence the radiosensitivity of normal tissue. It has been demonstrated that S1P administration prevents irradiation-induced ovarian failure by inhibiting apoptosis (39, 40) and protects mice from radiation-induced gastrointestinal syndrome (31), suggesting that S1P signaling may play an important role in the radiation response in normal tissue. Thus, future preclinical studies will need to investigate the effects of FTY720 on radiosensitivity of normal tissue, before clinical testing.

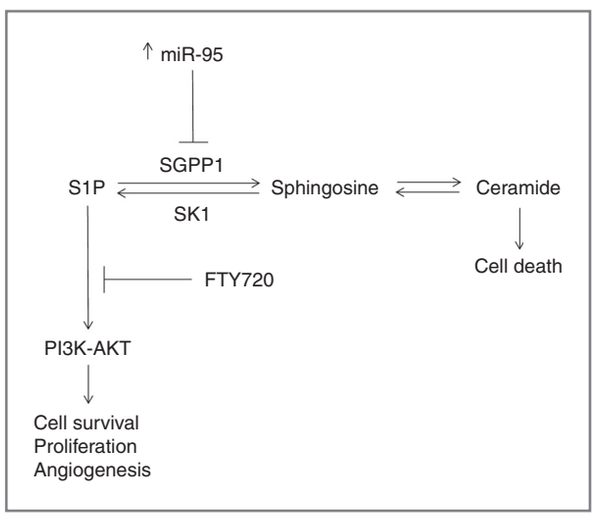

Figure 7. Proposed model of miR-95 action on cell survival by targeting SGPP1. The balance between cell survival and cell death signals is partly regulated by the levels of sphingosine-1-phosphate (S1P) and sphingosine. Sphingosine kinase 1 (SK1) phosphorylates sphingosine to form S1P, whereas SGPP1 dephosphorylates S1P to sphingosine. miR-95 overexpression in cancer cells downregulates SGPP1 expression, which promotes increased S1P signaling, PI3K-AKT pathway activation, resulting in increased cell survival, proliferation, and angogenesis. FTY720 inhibits S1P signaling and thus sensitizes miR-95 overexpressing cells to cell death.

Our xenograft tumor experiments revealed that miR-95 overexpressing tumors have less necrosis and increased proliferation, particularly following ionizing radiation. This is reflective of our *in vitro* findings, where miR-95 overexpression improves radiation clonogenic survival, increases the percentage of cells able to bypass an ionizing radiation–induced G_2–M checkpoint, and promotes cellular proliferation. We observed increased MVD in irradiated PC3-miR-95 tumors compared with PC3-control tumors indicative of increased angiogenesis. This suggests that in addition to direct tumor effects, miR-95 may modify the tumor microenvironment by increasing angiogenesis to confer further survival of tumor cells after ionizing radiation. Other reports have suggested that S1P signaling via S1PR1 can enhance angiogenesis through a paracrine manner (i.e., secreted S1P acting upon endothelial cells), and can also lead to secretion of proangiogenic factors (41, 42).

Although SGPP1 seems to largely account for the radiation-resistant phenotype induced by miR-95, there are other aspects to miR-95 action that seem to act independently of SGPP1. For instance, knockdown of SGPP1 did not recapitulate invasiveness (data not shown), suggesting that other gene targets downstream of miR-95 mediate this effect. Overexpression of certain miRs are known to increase invasiveness and metastatic potential *in vivo* (43), in keeping with the pleotropic effects of miR-95. We hypothesize that miR-95 overexpression will increase metastatic potential, and we plan to test this in our future research using metastatic models.

miR-95 is unlikely to be the sole mechanism through which radiation resistance arises in all cell types. miR expression are known to differ between cell types, and thus the contribution of

Published OnlineFirst October 21, 2013; DOI: 10.1158/0008-5472.CAN-13-1657

a given miR to the cellular phenotype will likely vary. For instance, although miR-95 promotes radiation resistance, the extent to which this occurred varied in different cell types (e.g., RPF 1.28 in PC3 cells, but 1.13 in MDA-MB-231 cells). This highlights the importance of identifying and characterizing additional miRs that may be involved in radiation response, as well as other mechanisms that regulate the expression of a given miR. In searching for novel candidate miRs, our research has identified miR-92a, miR-18b, and miR-365 family members that are enriched in radiation-resistant cancer cells, and research is ongoing to test their potential role in cancer radiation response. Recently published reports highlight their oncogenic and prognostic potential. For instance, miR-92a promotes esophageal cancer cell migration and invasion *in vitro*, and high expression of miR-92a correlates with lymph node metastases and poor overall survival in esophageal squamous cell carcinoma and colorectal carcinoma (44–46). Similarly, miR-18b overexpression promotes proliferation and loss of cell adhesion, and elevated levels of this miR correlates with reduced relapse-free survival in hepatocellular carcinoma (47). Finally, miR-365 expression is increased in breast cancer, as well as in response to UVB radiation (48, 49).

To our knowledge, there are no published clinical reports on miR and their role in predicting prostate cancer response to external beam radiotherapy or brachytherapy. We have found that miR-95 is significantly upregulated in prostate cancer samples compared with normal prostate. Based upon our findings here, we hypothesize that elevated tumor expression of miR-95 could contribute toward the prediction of a poor response to radiation treatment and will be the focus for future translational studies.

In conclusion, our research highlights the utility of our model in the discovery of miRs relevant to radiation resistance, and demonstrates for the first time, the ability of miR-95 to promote cancer radiation resistance through targeting of SGPP1.

Disclosure of Potential Conflicts of Interest

No potential conflicts of interest were disclosed.

Authors' Contributions

Conception and design: X. Huang, C.S. Wong, F.-F. Liu, S.K. Liu
Development of methodology: X. Huang, S. Taeb, S.K. Liu
Acquisition of data (provided animals, acquired and managed patients, provided facilities, etc.): X. Huang, S. Taeb, U. Emmenegger, E. Korpela, C.S. Wong
Analysis and interpretation of data (e.g., statistical analysis, biostatistics, computational analysis): X. Huang, S. Taeb, S. Jahangiri, U. Emmenegger, E. Tran, J. Bruce, C.S. Wong, F.-F. Liu, S.K. Liu
Writing, review, and/or revision of the manuscript: X. Huang, S. Taeb, U. Emmenegger, A. Mesci, E. Korpela, D. Vesprini, C.S. Wong, R.G. Bristow, S.K. Liu
Administrative, technical, or material support (i.e., reporting or organizing data, constructing databases): X. Huang, S. Taeb, S. Jahangiri, C.S. Wong, S.K. Liu
Study supervision: X. Huang, S.K. Liu

Acknowledgments

The authors thank C. Leoveanu for her excellent technical assistance. The authors thank Y. Amemiya at the Sunnybrook Genomics Core Facility for his excellent technical assistance with next-generation sequencing. The authors also thank The Centre for Applied Genomics for their expert gene array service.

Grant Support

This research was supported by Prostate Cancer Canada (PCC; S.K. Liu is a PCC Clinician-Scientist) and is proudly funded by the Movember Foundation—Grant No. D2013-24, the Ontario Institute for Cancer Research (OICR), the Canada Foundation for Innovation-MEDI ORF, the Motorcycle Ride for Dad (Huronia branch), and the Dean's Fund (Faculty of Medicine, University of Toronto). A. Mesci is supported by the CREMS Research Scholar Program (Faculty of Medicine, University of Toronto). E. Korpela is supported by a Canadian Institutes of Health Research (CIHR) fellowship. The contributions of U. Emmenegger and E. Tran were supported by an operating grant from PCC to U. Emmenegger.

The costs of publication of this article were defrayed in part by the payment of page charges. This article must therefore be hereby marked *advertisement* in accordance with 18 U.S.C. Section 1734 solely to indicate this fact.

Received June 12, 2013; revised August 29, 2013; accepted September 25, 2013; published OnlineFirst October 21, 2013.

References

1. Grossfeld GD, Olumi AF, Connolly JA, Chew K, Gibney J, Bhargava V, et al. Locally recurrent prostate tumors following either radiation therapy or radical prostatectomy have changes in Ki-67 labeling index, p53 and Bcl-2 immunoreactivity. J Urol 1998;159:1437–43.
2. Siders DB, Lee F. Histologic changes of irradiated prostatic carcinoma diagnosed by transrectal ultrasound. Hum Pathol 1992;23:344–51.
3. Leibovici D, Chiong E, Pisters LL, Guo CC, Ward JF, Andino L, et al. Pathological characteristics of prostate cancer recurrence after radiation therapy: implications for focal salvage therapy. J Urol 2012;188:98–102.
4. Iorio MV, Croce CM. MicroRNA dysregulation in cancer: diagnostics, monitoring and therapeutics: a comprehensive review. EMBO Mol Med 2012;4:143–59.
5. Lim LP, Lau NC, Garrett-Engele P, Grimson A, Schelter JM, Castle J, et al. Microarray analysis shows that some microRNAs downregulate large numbers of target mRNAs. Nature 2005;433:769–73.
6. Calin GA, Sevignani C, Dumitru CD, Hyslop T, Noch E, Yendamuri S, et al. Human microRNA genes are frequently located at fragile sites and genomic regions involved in cancers. Proc Natl Acad Sci U S A 2004;101:2999–3004.
7. Esquela-Kerscher A, Slack FJ. Oncomirs—microRNAs with a role in cancer. Nat Rev Cancer 2006;6:259–69.
8. Weidhaas JB, Babar I, Nallur SM, Trang P, Roush S, Boehm M, et al. MicroRNAs as potential agents to alter resistance to cytotoxic anticancer therapy. Cancer Res 2007;67:11111–6.
9. Niemoeller OM, Niyazi M, Corradini S, Zehentmayr F, Li M, Lauber K, et al. MicroRNA expression profiles in human cancer cells after ionizing radiation. Radiat Oncol 2011;6:29.
10. Metheetrairut C, Slack FJ. MicroRNAs in the ionizing radiation response and in radiotherapy. Curr Opin Genet Dev 2013;23:12–19.
11. Francia S, Michelini F, Saxena A, Tang D, de Hoon M, Anelli V, et al. Site-specific DICER and DROSHA RNA products control the DNA-damage response. Nature 2012;488:231–5.
12. Zhang X, Wan G, Berger FG, He X, Lu X. The ATM kinase induces microRNA biogenesis in the DNA damage response. Mol Cell 2011;41:371–83.
13. Lee KM, Choi EJ, Kim IA. microRNA-7 increases radiosensitivity of human cancer cells with activated EGFR-associated signaling. Radiother Oncol 2011;101:171–6.
14. Ng WL, Yan D, Zhang X, Mo Y-Y, Wang Y. Over-expression of miR-100 is responsible for the low-expression of ATM in the human glioma cell line: M059J. DNA Repair 2010;9:1170–5.
15. Huang Z, Huang S, Wang Q, Liang L, Ni S, Wang L, et al. MicroRNA-95 promotes cell proliferation and targets sorting Nexin 1 in human colorectal carcinoma. Cancer Res 2011;71:2582–9.

Published OnlineFirst October 21, 2013; DOI: 10.1158/0008-5472.CAN-13-1657

16. Zhang Y, Li M, Wang H, Fisher WE, Lin PH, Yao Q, et al. Profiling of 95 microRNAs in pancreatic cancer cell lines and surgical specimens by real-time PCR analysis. World J Surg 2009;33:698–709.
17. Li WG, Yuan YZ, Qiao MM, Zhang YP. High dose glargine alters the expression profiles of microRNAs in pancreatic cancer cells. World J Gastroenterol 2012;18:2630–9.
18. Liu SK, Bham SA, Fokas E, Beech J, Im J, Cho S, et al. Delta-like ligand 4-notch blockade and tumor radiation response. J Natl Cancer Inst 2011;103:1778–98.
19. Shi W, Gerster K, Alajez NM, Tsang J, Waldron L, Pintilie M, et al. MicroRNA-301 mediates proliferation and invasion in human breast cancer. Cancer Res 2011;71:2926–37.
20. De Bacco F, Luraghi P, Medico E, Reato G, Girolami F, Perera T, et al. Induction of MET by ionizing radiation and its role in radioresistance and invasive growth of cancer. J Natl Cancer Inst 2011;103:645–61.
21. Brown BD, Naldini L. Exploiting and antagonizing microRNA regulation for therapeutic and experimental applications. Nat Rev Genet 2009; 10:578–85.
22. Arora H, Qureshi R, Jin S, Park A-K, Park W-Y. miR-9 and let-7g enhance the sensitivity to ionizing radiation by suppression of NF-κB1. Exp Mol Med 2011;43:298–304.
23. Gupta AK, Bakanauskas VJ, Cerniglia GJ, Cheng Y, Bernhard EJ, Muschel RJ, et al. The ras radiation resistance pathway. Cancer Res 2001;61:4278–82.
24. Friedman RC, Farh KK-H, Burge CB, Bartel DP. Most mammalian mRNAs are conserved targets of microRNAs. Genome Res 2009; 19:92–105.
25. Kraemer A, Anastasov N, Angermeier M, Winkler K, Atkinson MJ, Moertl S. MicroRNA-mediated processes are essential for the cellular radiation response. Radiat Res 2011;176:575–86.
26. Zage PE, Sirisaengtaksin N, Liu Y, Gireud M, Brown BS, Palla S, et al. UBE4B levels are correlated with clinical outcomes in neuroblastoma patients and with altered neuroblastoma cell proliferation and sensitivity to epidermal growth factor receptor inhibitors. Cancer 2013;119:915–23.
27. Johnson KR, Johnson KY, Becker KP, Bielawski J, Mao C, Obeid LM. Role of human sphingosine-1-phosphate phosphatase 1 in the regulation of intra- and extracellular sphingosine-1-phosphate levels and cell viability. J Biol Chem 2003;278:34541–7.
28. Carlucci A, Porpora M, Garbi C, Galgani M, Santoriello M, Mascolo M, et al. PTPD1 supports receptor stability and mitogenic signaling in bladder cancer cells. J Biol Chem 2010;285:39260–70.
29. Pchejetski D, Bohler T, Stebbing J, Waxman J. Therapeutic potential of targeting sphingosine kinase 1 in prostate cancer. Nat Rev Urol 2011;8:569–678.
30. Mandala SM, Thornton R, Galve-Roperh I, Poulton S, Peterson C, Olivera A, et al. Molecular cloning and characterization of a lipid phosphohydrolase that degrades sphingosine-1-phosphate and induces cell death. Proc Natl Acad Sci U S A 2000;97:7859–64.
31. Bonnaud S, Niaudet C, Legoux F, Corre I, Delpon G, Saulquin X, et al. Sphingosine-1-phosphate activates the AKT pathway to protect small intestines from radiation-induced endothelial apoptosis. Cancer Res 2010;70:9905–15.
32. Fyles AW, McCready DR, Manchul LA, Trudeau ME, Merante P, Pintilie M, et al. Tamoxifen with or without breast irradiation in women 50 years of age or older with early breast cancer. N Engl J Med 2004;351:963–70.
33. Nava VE, Cuvillier O, Edsall LC, Kimura K, Milstien S, Gelmann EP, et al. Sphingosine enhances apoptosis of radiation-resistant prostate cancer cells. Cancer Res 2000;60:4468–74.
34. Brizuela L, Ader I, Mazerolles C, Bocquet M, Malavaud B, Cuvillier O. First evidence of sphingosine 1-phosphate lyase protein expression and activity downregulation in human neoplasm: implication for resistance to therapeutics in prostate cancer. Mol Cancer Ther 2012; 11:1841–51.
35. Helleman J, Jansen MP, Span PN, van Staveren IL, Massuger LF, Meijer-van Gelder ME, et al. Molecular profiling of platinum resistant ovarian cancer. Int J Cancer 2006;118:1963–71.
36. Cohen JA, Barkhof F, Comi G, Hartung HP, Khatri BO, Montalban X, et al. Oral fingolimod or intramuscular interferon for relapsing multiple sclerosis. N Engl J Med 2010;362:402–15.
37. Kappos L, Radue EW, O'Connor P, Polman C, Hohlfeld R, Calabresi P, et al. A placebo-controlled trial of oral fingolimod in relapsing multiple sclerosis. N Engl J Med 2010;362:387–401.
38. Pchejetski D, Bohler T, Brizuela L, Sauer L, Doumerc N, Golzio M, et al. FTY720 (Fingolimod) sensitizes prostate cancer cells to radiotherapy by inhibition of sphingosine kinase-1. Cancer Res 2010; 70:8651–61.
39. Paris F, Perez GI, Fuks Z, Haimovitz-Friedman A, Nguyen H, Bose M, et al. Sphingosine 1-phosphate preserves fertility in irradiated female mice without propagating genomic damage in offspring. Nat Med 2002;8:901–2.
40. Morita Y, Perez GI, Paris F, Miranda SR, Ehleiter D, Haimovitz-Friedman A, et al. Oocyte apoptosis is suppressed by disruption of the acid sphingomyelinase gene or by sphingosine-1-phosphate therapy. Nat Med 2000;6:1109–14.
41. Visentin B, Vekich JA, Sibbald BJ, Cavalli AL, Moreno KM, Matteo RG, et al. Validation of an anti-sphingosine-1-phosphate antibody as a potential therapeutic in reducing growth, invasion, and angiogenesis in multiple tumor lineages. Cancer Cell 2006;9:225–38.
42. Chae SS, Paik JH, Furneaux H, Hla T. Requirement for sphingosine 1-phosphate receptor-1 in tumor angiogenesis demonstrated by *in vivo* RNA interference. J Clin Invest 2004;114:1082–9.
43. Ma L, Teruya-Feldstein J, Weinberg RA. Tumour invasion and metastasis initiated by microRNA-10b in breast cancer. Nature 2007;449: 682–8.
44. Tsuchida A, Ohno S, Wu W, Borjigin N, Fujita K, Aoki T, et al. miR-92 is a key oncogenic component of the miR-17–92 cluster in colon cancer. Cancer Sci 2011;102:2264–71.
45. Chen Z-l, Zhao X-h, Wang J-w, Li B-z, Wang Z, Sun J, et al. microRNA-92a promotes lymph node metastasis of human esophageal squamous cell carcinoma via E-cadherin. J Biol Chem 2011; 286:10725–34.
46. Zhou T, Zhang G, Liu Z, Xia S, Tian H. Overexpression of miR-92a correlates with tumor metastasis and poor prognosis in patients with colorectal cancer. Int J Colorectal Dis 2013;28:19–24.
47. Murakami Y, Tamori A, Itami S, Tanahashi T, Toyoda H, Tanaka M, et al. The expression level of miR-18b in hepatocellular carcinoma is associated with the grade of malignancy and prognosis. BMC Cancer 2013;13:99.
48. Yan L-X, Huang X-F, Shao Q, Huang M-Y, Deng L, Wu Q-L, et al. MicroRNA miR-21 overexpression in human breast cancer is associated with advanced clinical stage, lymph node metastasis and patient poor prognosis. RNA 2008;14:2348–60.
49. Guo L, Huang Z-X, Chen X-W, Deng Q-K, Yan W, Zhou M-J, et al. Differential expression profiles of microRNAs in NIH3T3 cells in response to UVB irradiation. Photochem Photobiol 2009;85: 765–73.

Published OnlineFirst October 21, 2013; DOI: 10.1158/0008-5472.CAN-13-1657

Cancer Research
The Journal of Cancer Research (1916–1930) | The American Journal of Cancer (1931–1940)

AACR American Association for Cancer Research

miRNA-95 Mediates Radioresistance in Tumors by Targeting the Sphingolipid Phosphatase SGPP1

Xiaoyong Huang, Samira Taeb, Sahar Jahangiri, et al.

Cancer Res 2013;73:6972-6986. Published OnlineFirst October 21, 2013.